JGR Atmospheres

RESEARCH ARTICLE
10.1029/2019JD030835

Episodes of Warm-Air Advection Causing Cloud-Surface Decoupling During the MARCUS

Youtong Zheng[1] and Zhanqing Li[1]

[1]Earth System Science Interdisciplinary Center, University of Maryland, College Park, MD, USA

Key Points:
- Ship data over the Southern Ocean are used to examine the response of a cloud-topped boundary layer (CTBL) to warm air advection (WAA)
- CTBL becomes highly stratified under the influence of WAA, the degree of which is greater than subtropical decoupled CTBLs
- The strong stratification suppresses the growth of cumulus clouds so that the cumulus-coupled CTBLs typical in subtropics do not exist

Correspondence to:
Y. Zheng,
zhengyoutong@gmail.com

Citation:
Zheng, Y., & Li, Z. (2019). Episodes of warm-air advection causing cloud-surface decoupling during the MARCUS. *Journal of Geophysical Research: Atmospheres*, *124*. https://doi.org/10.1029/2019JD030835

Received 18 APR 2019
Accepted 21 SEP 2019
Accepted article online 22 OCT 2019

Abstract It has been known for decades that advection of a cloud-topped marine boundary layer (CTBL) over warmer sea surface causes the stratification (or decoupling) of the CTBL via the entrainment feedback, a mechanism commonly known as "deepening-warming" decoupling that is typical in subtropics. This study focuses on the opposite direction of advection, that is, low-level warm air advection (LLWAA), and its impacts on the decoupling degree of a CTBL. Our hypothesis is that LLWAA stabilizes a CTBL, causing a decoupling of the CTBL. It is tested for three LLWAA episodes observed during the Measurements of Aerosols, Radiation, and CloUds over the Southern Ocean (MARCUS) field campaign between the Hobart (43°S, 147°E), Australia, and several Antarctic coast stations. By synthesizing the shipborne measurements of CTBL structure, Himawari-8 satellite imagery of cloud fields, and reanalysis of meteorological field, four common characteristics of CTBLs under the LLWAA are found: (1) CTBLs are highly stratified to the extent that penetrations of cumulus into main temperature inversions, which are common for subtropical decoupled CTBLs, do not exist; (2) sea surface temperature is 1–2 K lower than the near-surface air temperature; (3) clouds manifest stratiform with lifetime as long as several tens of hours; and (4) they locate in warm sectors of middle-latitude cyclones. Possible mechanisms for the maintenance of decoupled clouds under LLWAA are discussed in terms of dynamic and thermodynamic factors. Lapse rates of the decoupled CTBLs are markedly lower than those commonly used for passive satellite estimation of cloud top heights.

1. Introduction

How marine boundary-layer (MBL) clouds respond to global warming remains a major source of uncertainty that limits the accuracy of projections of future climate (Boucher et al., 2013). The persistent presence of MBL clouds is largely controlled by the degree they are coupled with surface fluxes (Wood, 2012). Our theoretical understanding of the surface-cloud coupling in a MBL is largely based on, if not originated from, Lilly (1968)'s seminal mixed-layer model that has been widely considered as the simplest authentic description of a cloud-topped MBL (Stevens, 2006). A key assumption underlying Lily's model is that a cloud-topped MBL is always well mixed with vertically uniform moist conserved variables (e.g., liquid water potential temperature and total water vapor mixing ratio). This well-mixed state of the MBL is conventionally called "coupled" and, on the contrary, a state deviated from the well-mixed state (e.g., vertical stratification of moist conserved variables) is called "decoupled" (Bretherton & Wyant, 1997; Dong et al., 2015; Jones et al., 2011; McGibbon & Bretherton, 2017; Nicholls, 1984; Stevens, 2000; Zheng et al., 2018a).

What causes the MBL decoupling can be understood from a perspective of energetics of a MBL. A coupled stratocumulus (Sc)-topped MBL is maintained by an energy exchange between the turbulent kinetic energy (TKE) and the potential energy of the mean fluid. TKE generated by cloud-top radiative cooling or surface buoyancy fluxes is transformed to the potential energy for sustaining a well-mixed state. Decoupling occurs when the TKE is not adequate for supplying the energy needed for well mixing the MBL. This energetic perspective classifies decoupling mechanisms into two categories: (1) decrease in the TKE supply and (2) increase in the demand for TKE for maintaining "well-mixedness." The former primarily refers to the weakening in cloud-top radiative cooling such as the insolation-induced decoupling of MBL during daytime (Nicholls, 1984). The later includes the precipitation-induced stabilization (Wood, 2012) and the deepening of a Sc-topped MBL that ventilates warm free-tropospheric air into the MBL (Bretherton & Wyant, 1997), a TKE-consumption process.

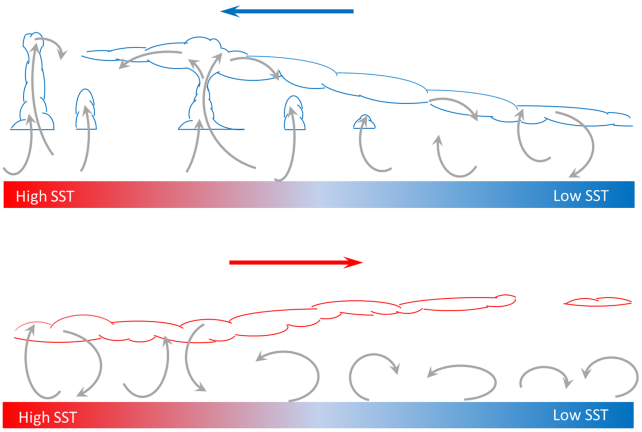

Figure 1. Schematic diagram of response of MBL coupling state to the external forcing of thermal advection. Adapted from Zheng et al. (2018b).

These decoupling mechanisms have been extensively studied by field campaign observations and numerical simulations, but the majority of these studies are for subtropical environments where MBLs are advected over warmer sea water (Figure 1a). The cold thermal advection allows the MBL to remain convective so that the decoupled layer (the layer between surface mixed layer and the elevated Sc cloud base) is often conditionally unstable (Wood & Bretherton, 2004). This allows the underlying cumulus clouds to penetrate through the decoupled layer and feed the decoupled Sc decks, forming a cumulus-coupled MBL. This is the reason why decoupled MBLs are often more precipitating than the coupled MBLs due to the deep cumuliform clouds (Martin et al., 1995; O et al., 2018; Zheng et al., 2018a). This mechanism, however, is unlikely to be present under low-level warm air advections (LLWAA; Figure 1b). Being advected over colder sea surfaces, the subcloud layer is stable, which is unfavorable for the vertical development of cumulus clouds. The coupling properties of MBLs under such LLWAA have been less studied in comparison with those in low-level cold air advections (LLCAA). Possible reasons for the unpopularity are twofold. First, among regions where extensive Sc decks occur, the semipermanent Sc sheets near west of the subtropical continents have been receiving the most attention because of the climatologically high cloud coverage and the strong solar illumination. Thus, previous field experiments are concentrated near these regions where LLWAA samples are scarce due to the prevalence of cold ocean currents. Second, satellite data have been used to associate the cloud properties with horizontal thermal advections (Agee, 1987; Muhlbauer et al., 2014; Norris & Iacobellis, 2005; Wall et al., 2017), but satellite observations do not portray the coupling detail of a MBL. Although this issue is being moderated by the advent of active satellite sensors that profile the vertical structures of MBLs (Goren et al., 2018; Luo et al., 2016), the vertical resolution is poor given the shallowness of MBLs. In practice, the only accurate way to characterize the coupling state of a MBL is through field experiments equipped with adequate instrumentation.

Southern Ocean is a region where LLWAA frequently occurs (Wall et al., 2017). Extratropical cyclones drive southward advections of air masses in the warm sectors of the cyclones, causing the LLWAA. Also, previous field campaigns document frequent occurrence of decoupled MBLs over this region (Chubb et al., 2016; Hande et al., 2012; Jensen et al., 2000; Russell et al., 1998). For example, during the Aerosol Characterization Experiment (ACE-1), Russell et al. (1998) document a MBL with two-layer structure: a classical well-mixed lower layer and, on top of it, a less-well-mixed layer with intermittent occurrence of clouds. A strong inversion was found on top of the second layer. MBLs with similar two-layer structure were also found in Southern Ocean Cloud Experiments (SOCEX; Boers et al., 1998; Jensen et al., 2000), High-performance Instrumented Airborne Platform for Environmental Research (HIAPER) Pole-to-Pole Observations (HIPPO; Chubb et al., 2016), and a long-term ground site on the Macquarie Island (Hande et al., 2012). These previous works have various focuses, but none of them was dedicated to a detailed examination of the contribution of LLWAA to the decoupled MBLs. This motivates the present study. We tackle this problem by using shipborne observations during the Measurements of Aerosols, Radiation, and CloUds over the Southern Ocean (MARCUS) field campaign. As one of the world's most pristine regions, Southern Ocean is an ideal region for studying the aerosol cloud-mediated effect because of the sublinear dependence of cloud albedo on aerosol perturbations (Carslaw et al., 2013). Given that the MBL decoupling degree modulates the pathway through which surface-generated aerosols reach cloud bases, an improved understanding of the LLWAA-driven MBL decoupling should help understand the aerosol cloud-mediated effect and its climatic impacts.

Data and methodology are described in the next section. A total of three episodes of MBL clouds under the influence of distinctive LLWAA are found during the MARCUS. Section 3 shows case studies for each LLWAA event, for which shipborne, satellite imagery, and reanalysis data are synthesized to examine the key properties of the cloud-topped MBLs under the influence of LLWAA. Section 4 summarizes the findings and discusses their implications.

2. Data and Methods

2.1. MARCUS Observations

The MARCUS field campaign is a six-month-long ship-based field experiment conducted between the Australia and the Antarctic. An Australian vessel, *Aurora Australis*, carries the U.S. Department of Energy Atmospheric Radiation Measurement (ARM) Climate Research Facility's second Mobile Facility (AMR2), routinely travelling between the Hobart (43°S, 147°E), Australia, and several Antarctic coast stations: Mawson (67.6°S, 62.9°E), Davis (68.6°S, 78.0°E), and Casey (66.3°S, 110.8°E). Each transit between the Antarctic and the Hobart lasts around two weeks.

The Marine W-Band (95 GHz) ARM Cloud Radar (MWACR), a vertically pointing Doppler radar operating at 95 GHz, is used to detect cloud boundaries. Cloud-base heights are measured by a Vaisala Ceilometer. Surface meteorological measurements including the near-surface air temperature (T_{air}), relative humidity, and pressure are used to calculate the lifting condensation level using the analytic formula from Romps (2017). An Infrared Thermometer is used to measure the sea surface temperature (SST). Radiosondes were launched from the ship 4 times per day. We determine the height of the inversion-layer base (z_{inv}) by finding the altitude where the temperature minimizes below the altitude with the strongest temperature inversion. Surface precipitation rate is obtained from an optical rain gauge (ORG). The ORG works poorly when the temperature is below 0 °C, which does not affect our analysis because all the three episodes have $T_{air} > 0$ °C. There are about four-month worth of data with most of these instruments functional.

2.2. Himawari-8 Imagery and Reanalysis Data

Satellite imagery data from the Advanced Himawari Imager onboard the Himawari-8 are used to examine the spatial distribution of clouds and their types. We generate multispectral red-green-blue (RGB) composites by combining multiple channels. During the daytime, the conventional "Daytime Microphysical RGB" scheme (*Daniel* Rosenfeld & Lensky, 1998) is used. The red, green, and blue components are modulated by the radiances of 0.64, 1.6, and 10.8 μm, respectively. The radiances of these three channels are qualitative measures of the cloud optical depth and cloud water/ice amount (redder for optically thicker clouds), cloud particle size and phase (greener for clouds with smaller particles), and temperature (bluer for cold objects), respectively. During the nighttime when solar radiation is absent, we use the "Nighttime Microphysical RGB" instead (Lensky & Rosenfeld, 2008). The red component is modulated by the brightness temperature difference between the 12.4- and 10.4-μm channels, which, similar to 0.64-μm reflectance, is a measure of clouds' opaqueness (Inoue, 1987). The green component is regulated by the brightness temperature difference between the 10.4- and 3.9-μm channels, which is sensitive to cloud particle size and phase (greener for water clouds with smaller droplets). The blue component is modulated by 10.4 μm. Table 1 summarizes the receipt for multispectral composition of the two RGB schemes and shows examples of identifying the ocean surface and different types of clouds.

2.3. Reanalysis Data and Backward Trajectory

The European Centre for Medium-Range Weather Forecasts (ECMWF) Interim reanalysis data are used to create maps of synoptic meteorology. The reanalysis variables include SST, sea surface pressure, 10-m wind speed, and vertical velocity at 700 hPa. The 0.5 × 0.5° Global Data Assimilation meteorology data are used to drive the Hybrid Single Particle Lagrangian Integrated Trajectory Model (HYSPLIT; Stein et al., 2015). The 36-hr backward trajectory computations are run on level of 500 m above the sea surface.

3. Results

We select LLWAA episodes by calculating the low-level horizontal temperature advection along the 36-hr backward trajectory for each air mass that passed through the *Aurora Australis*:

$$\overline{-\frac{dSST}{dt}} = \overline{-\mathbf{V}_{500\ m}\cdot\nabla SST} \tag{1}$$

where the $\mathbf{V}_{500\ m}$ is the horizontal wind at 500 m, consistent with the altitude chosen in HYSPLIT simulations. The overbar does not stand for simple average, but the best fit trend of SST along the trajectory during

Table 1
Receipts for the Multispectral Composition of Daytime and Nighttime Microphysical RGB and Typical Examples

	Color beam	Channel	Range	Example
Daytime Microphysical RGB	Red	0.64 μm	0–1	*Ocean surface:* blue
	Green	1.6 μm	0–0.8	*Low clouds:* pastel or whitish green, sometimes pinkish
	Blue	10.4 μm	203–323 K	*Cirrus/high thick clouds:* orange/red-orange
Nighttime Microphysical RGB[a]	Red	12.4–10.4 μm	−6.7–2.6 K	*Ocean surface:* magenta or blue
	Green	10.4–3.9 μm	−3.1–5.2 K	*Low clouds:* pastel or whitish green
	Blue	10.4 μm	243.6–292.6 K	*Cirrus/high thick clouds:* black/dark red

[a]The receipt is based on the *Shimizu* (2015) who adjusted conventional standard thresholds of RGB of operational European Organisation for the Exploitation of Meteorological Satellites (EUMETSAT). The adjusted receipts account for the spectral characteristics differences so that the visualization from the Himawari-8 RGB imagery is consistent with that from the legacy EUMETSAT.

the past 36 hr. Low cloud samples (cloud top <3 km) with at least six continuous hours of $-\overline{\frac{dSST}{dt}}>1$ K/day are selected as LLWAA events. A total of three episodes of LLWAA with a combined period of ~70 hr were identified from the four-month worth of shipborne data. This occupies ~15% of the total low cloud samples. All the three episodes are located north of 50°S when the *Aurora Australis* were travelling to or departing from Hobart, Australia.

3.1. Case Study 1: 28 February–3 March 2018

From the 28 February through 3 March 2018, the *Aurora Australis* sampled cloud-topped MBLs that experienced dramatically different low-level thermal advections. This offers a good opportunity to examine the role of thermal advection in regulating the coupling state of a cloud-topped MBL. Figure 2a shows the ship track (red stars) and 36-hr backward trajectories from ship locations every 6 hr. The background shading represents the mean reanalysis SST during this four-day period. In the beginning, MBL air masses that passed by the *Aurora Australis* were from the west. They experienced little SST gradient during the $t = -36$–0 hr. After one day, the wind flow passing through the *Aurora Australis* started to shift from westerly to northwesterly, indicating the occurrence of LLWAA. Near the end of the period when the *Aurora Australis* approached Hobart, Australia, winds shifted to southwesterly direction, suggesting a switch from LLWAA to LLCAA. Figure 2b shows that the $-\overline{\frac{dSST}{dt}}$ started with weakly positive values and then increased dramatically after one day. The period of strong LLWAA lasted for approximately two days and then weakened, eventually shifting to strong LLCAA in the end. Next, we examine the characteristics of synoptic maps and the responses of MBLs to the changes in the temperature advection.

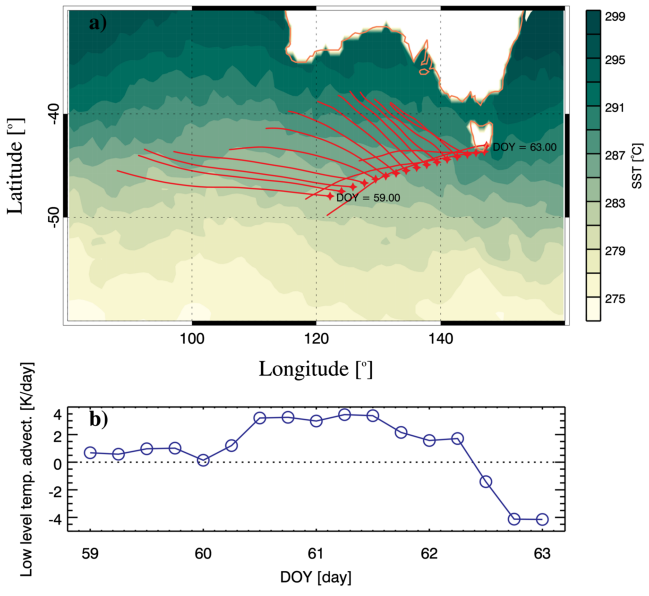

Figure 2. (a) SST map averaged between 28 February and 3 March 2018. *Aurora Australis* locations are marked by the red filled stars every 6 hr. Red lines mark the 36-hr back trajectories at 500 m with receptor points at *Aurora Australis*. (b) The evolution of the 36-hr low-level temperature advection for air masses went through the ship every 6 hr.

3.1.1. Synoptic Setting

Figures 3 and 4 show the synoptic settings and satellite daytime RGB imageries, respectively, throughout the course of the event. In the beginning (Figure 3a), the *Aurora Australis* (red star) located near the southern flank of a high-pressure system and was under the influence of the westerly wind. The upstream air masses experienced little SST variation before being sampled by the *Aurora Australis*. A low-pressure center in the southwest was developing, with a northwest-southeast cold front swirling toward the east. From the satellite imageries (Figures 4a and 5a), the clouds above the ship have extensive cloud coverage with mean visible reflectance of ~0.4. After 24 hr when the low-pressure center approached (Figure 3b), the cold front becomes more north-south. The northwesterly winds in front of the cold front brought warm and moist air masses southward over cold sea surfaces. The cloud fields manifest north-south stripes (Figure 4b). The clouds over the *Aurora Australis* (Figure 5b) are optically

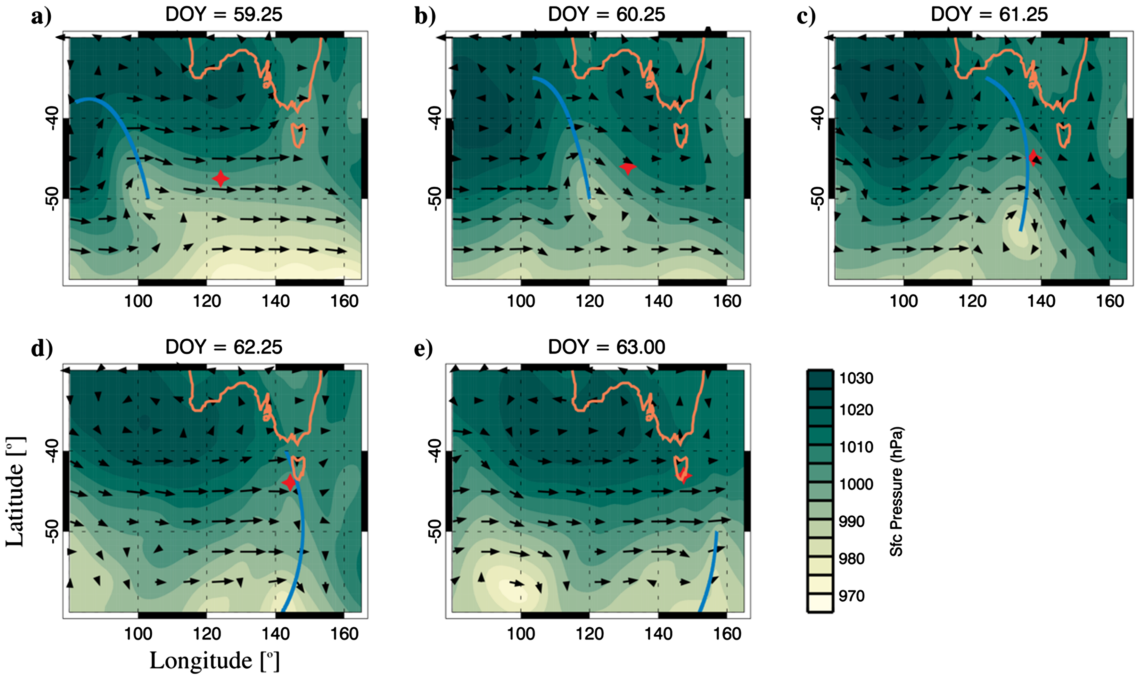

Figure 3. Mean sea level pressure at DOY (day of year) = (a) 59.25, (b) 60.25, (c) 61.25, (d) 62.25, and (e) 63.00 in 2018. Black arrows stand for the mean wind vectors at 10 m above the sea surface. The locations of the *Aurora Australis* are marked by the red filled stars. Blue solid lines mark the cold fronts that are determined manually.

thinner with smaller fractional coverage compared with the clouds passed through the ship 24 hr ago (Figure 5a). By tracking the same air masses along the −36–0-hr backward trajectory from satellite imageries (Animation S1), we found that the clouds experienced marked decrease in optical thickness and

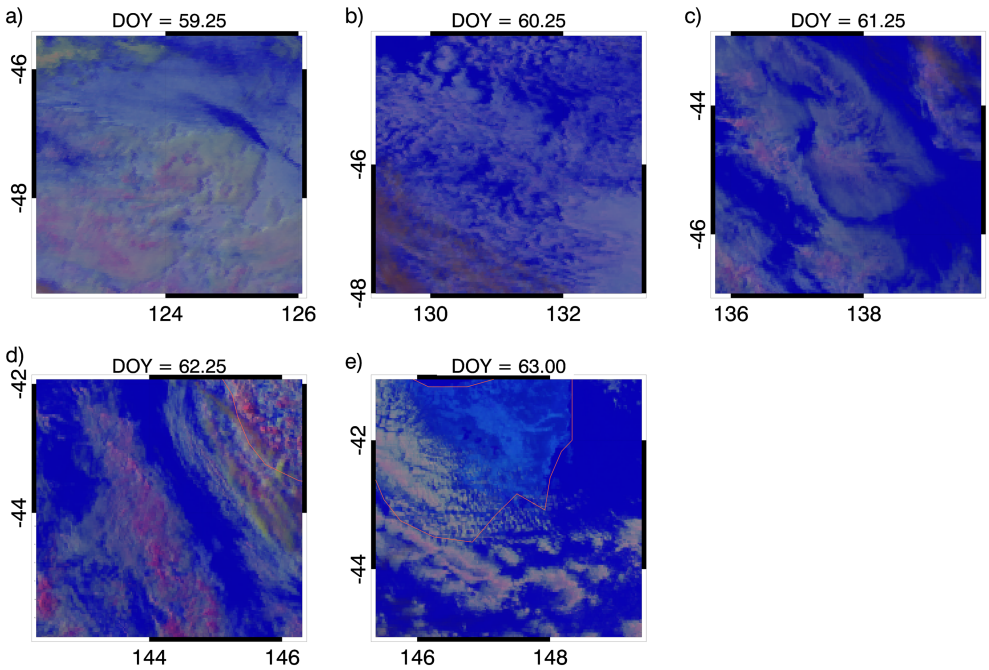

Figure 4. Himawari-8 "Day microphysical RGB" composite imageries at DOY = (a) 59.25, (b) 60.25, (c) 61.25, (d) 62.25, and (e) 63.00 in 2018. The locations of the *Aurora Australis* are marked by the red open circles. Orange solid lines mark the cold fronts that are determined manually.

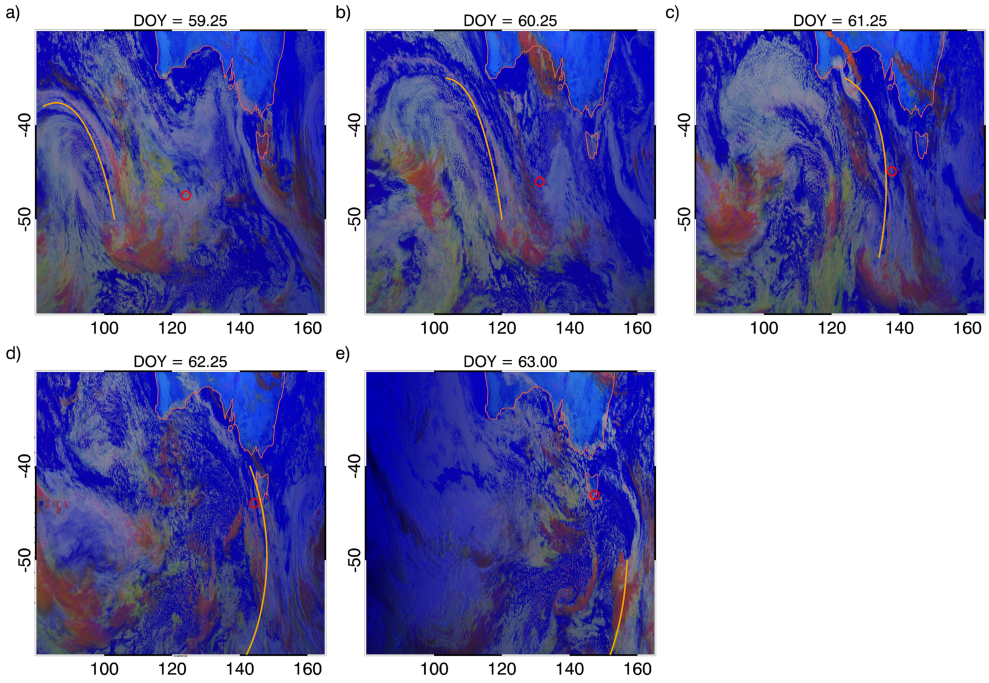

Figure 5. Same with Figure 4 but zoomed-in version with 2 × 2° region centered on the locations of *Aurora Australis*.

cloud fractional coverage during $t = -36$–0 hr when the cloud fields were experiencing marked LLWAA. This is consistent with previous studies suggesting that cloud fractional coverage and optical thickness are smaller in LLWAA conditions (George & Wood, 2010; Norris & Iacobellis, 2005; Wall et al., 2017; Xu et al., 2005).

After one day, the frontal system captured the *Aurora Australis* (Figure 3c). The ship was still undergoing northerly winds that advected upstream warm clouds over colder sea surfaces in the south. The cloud fields manifest anvil-like thin sheets (Figure 5c). There are some reddish regions (larger optical thickness) scattered within the white anvils. As will be shown in the shipborne radar image (Figure 6), these reddish areas are likely to be the shallow cumulus developed underneath the anvils. Because the subcloud layer is highly stable due to the LLWAA, the cumulus clouds were suppressed in the vertical, making them appear only slightly reddish.

The LLWAA persisted for approximately one day until the cold front had passed over the *Aurora Australis* (Figure 3d) and the LLWAA weakened. The satellite imagery (Figure 5d) shows that the clouds were optically thicker than those passing through the ship 24 hr ago. Eighteen hours later when the *Aurora Australis* arrived at the Hobart, Australia, winds shifted to southwesterly (Figure 4e). This caused a LLCAA that is favorable for the development of convective MBLs, which is visible from the satellite imageries (Figures 4e and 5e) showing scattered clusters of cumuliform clouds south of the ship.

3.2. MBL Decoupling

Figure 6a shows the MWACR height-time image of the MBLs during the event. The black and red points represent the ceilometer-measured cloud base heights and lifting condensation level (LCL), respectively. Profiles of potential temperature (θ) derived from the radiosonde data are also plotted (yellow lines). They are scaled by 6 hr (±3 hr centered on the radiosonde launching time) so that they can be overplotted on the radar image.

During the first ~24 hr when there is no distinctive thermal advection, well-mixed Sc-topped MBLs are noted: cloud bases overlapping with the LCL, Sc decks topped by pronounced temperature inversions, and vertically uniform θ from the surface to the base of the inversions. As the thermal advection becomes more positive (open blue circles in Figure 6c), the LCL becomes detached from the cloud bases. Increase

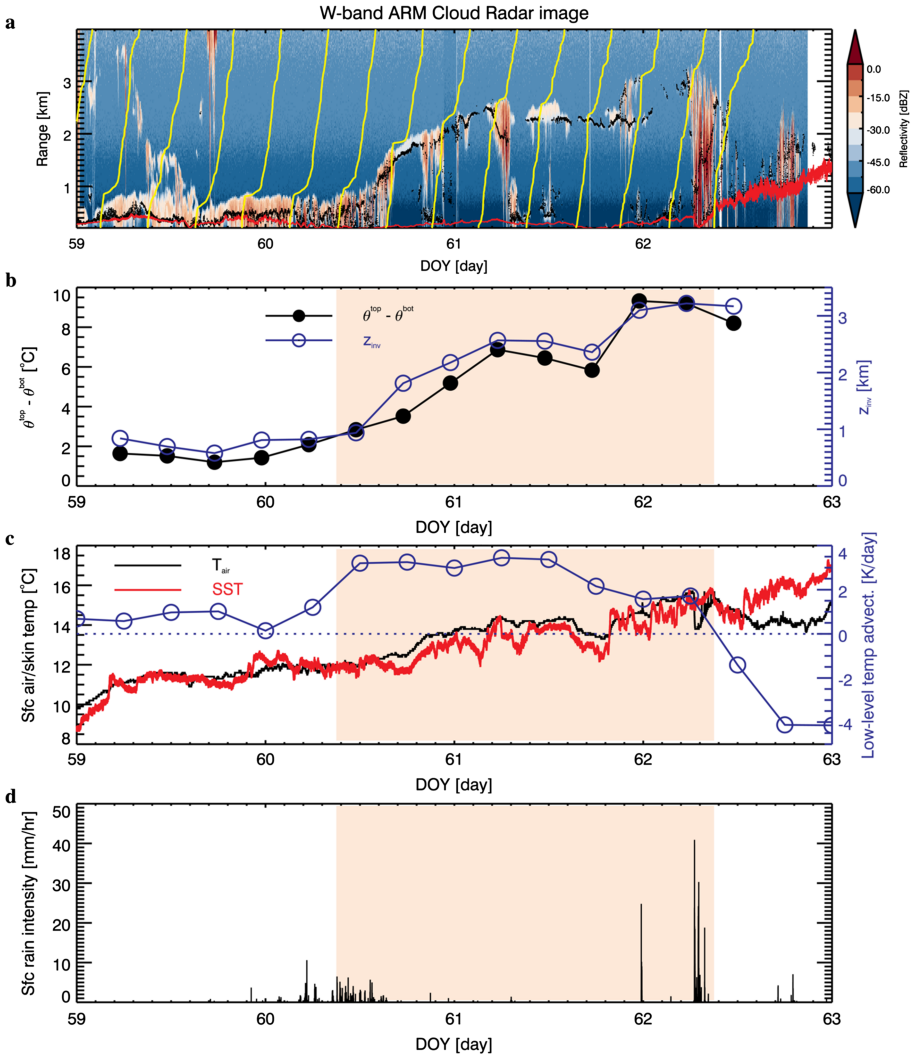

Figure 6. (a) Height-time plot of MWACR image during DOY = 59–63. The red, black, and yellow lines mark the LCL, ceilometer-measured cloud-base heights, and profiles of θ scaled by ±3 hr. (b) Time series of θ^{top}-θ^{bot} and z_{inv}; (c) T_{air}, SST, and low-level temperature advection; and (d) surface rain intensity measured by a rain gauge. Pink shadings mark the period with distinctive warm air advection ($-\overline{\frac{dSST}{dt}}>1$ K/day).

in the strength of LLWAA is accompanied by an increased difference between the bases of the Sc sheets below the main temperature inversion and the LCL, indicating a greater degree of decoupling. Cumulus clouds rooted from the surface layer are occasionally present underneath the decoupled Sc decks. They are very shallow primarily because of the stable subcloud layer under the LLWAA condition.

To quantify the decoupling degree of the MBLs, we use the θ^{top}-θ^{bot}, where the θ^{top} and θ^{bot} stand for the θ averaged through the top and bottom 25% of a MBL below z_{inv}. The θ^{top}-θ^{bot} remains relatively constant (1–2 K) on the first day and then increases considerably as the LLWAA starts to dominate (Figure 6b). The impacts of LLWAA on the MBL stratification can be clearly seen from the evolution of the difference between the SST and T_{air} (Figure 6c). The SST is close to T_{air} on the first day and then becomes 1–2 K smaller than T_{air} as the LLWAA becomes significant. A negative SST-T_{air} indicates negative surface heat fluxes, which inhibits the vertical mixing in the surface layer, promoting the MBL decoupling.

This finding is consistent with our hypothesis posed in the beginning of the manuscript: LLWAA contributes to the decoupling of a cloud-topped MBL. Our hypothesis is from a simple thermodynamic point of view: warm air over cold surfaces causes stratification. This hypothesis, however, does not account for the large-

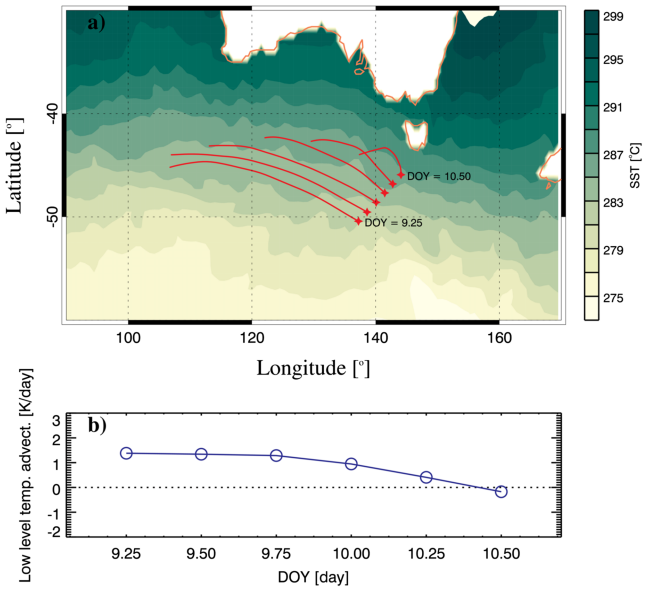

Figure 7. Same with Figure 2 but for DOY = 9.25–10.5.

scale air motion that is often tied with the low-level thermal advections (Holton, 1973). The reason why large-scale air motion is important for the MBL decoupling is that it determines the MBL depth (through conservation of mass). A deeper MBL is typically associated with a greater degree of decoupling (Wood & Bretherton, 2004; Zuidema et al., 2009). This could be understood from the perspective of TKE budget described in section 1. A deeper MBL requires more TKE for maintaining a well-mixed state. As a major source of turbulent energy in a cloud-topped MBL, the cloud top radiative cooling has an upper limit (Wood, 2012). Previous observations show that Sc-capped MBLs can hardly maintain well mixed when z_{inv} >1.1 km (Wood & Bretherton, 2004; Zheng et al., 2018b; Zuidema et al., 2009). If there is a significant large-scale ascent motion that elevates the z_{inv} above 1.1 km, the MBL has to be decoupled regardless of the thermal advection condition. According to the omega equation for synoptic scale fluid (Holton, 1973), LLWAA contributes to large-scale ascent motion. In our case, during the distinctive LLWAA period at DOY (day of year) = 60.5–62, the ship was situated in front of an approaching cold front system where the warm conveyer belts elevate air masses in the MBL (Sinclair et al., 2010) and enhances the MBL decoupling that was initiated by the LLWAA. This is apparent from the Figure S1 showing that the upstream region of the LLWAA period is dominantly controlled by synoptic ascent motions.

In addition to the large-scale vertical motion, frontal lifting (or "overrunning") may also contribute to the ascent because a LLWAA can also be considered as a weak warm front. A major difference between the synoptic-scale lifting and frontal lifting is that the former is a dynamic forcing mechanism constrained by the equation of continuity, whereas the latter is a pure kinematic process that operates on mesoscale. Separating them is practically challenging given the large uncertainty of the reanalysis over the remote ocean. Here we consider their combined effects as a whole, which is named as "dynamic lifting." The impact of dynamic lifting is suggested by the uncommonly deep z_{inv} (2–3 km). This can be understood from a thought experiment. We consider a well-mixed Sc-topped MBL with z_{inv} of 0.8 km, which is a typical value for a well-mixed MBL. Over subtropical oceans, the typical entrainment rate is ~0.4 cm/s (Faloona et al., 2005; Wood & Bretherton, 2004), which is likely to be larger than that in a LLWAA condition where a MBL is more stable and ineffective for ventilation. In the absence of dynamic lifting, entrainment deepens the MBL by ~1.04 km after 72 hr, giving z_{inv} = 1.84 km. This value is perhaps the upper bound of z_{inv} without the help of large-scale ascent because under a LLWAA condition the entrainment rate should be lower than the values typical of subtropical Sc decks. Thus, it is reasonable to conjecture that dynamic lifting elevated the cloud layers, further strengthening the decoupling of the MBL.

During the LLWAA period (DOY = 60.5–62), the clouds remain laminar and largely quiescent with weak drizzles near cloud bases (Figure 6a). There are occasional periods of marked drizzling at cloud bases, but a majority of them are evaporated before reaching the ground, as shown by the weak surface precipitation (<2 mm/hr) measured by the ship-borne rain gauge during the LLWAA period.

Near the end of the period, the low-level thermal advection switches from positive to negative (Figure 6c). The SST becomes higher than the T_{air} by several K, suggesting a more convective MBL. Driven by the convection, cumulus clouds start to form and grow deeper in the vertical, generating stronger precipitation relative to the LLWAA period (Figure 6d). The convection strengthens the vertical mixing of the surface layer, ventilating overlying dry air into the surface layer. This desiccates the boundary layer and markedly elevates the LCL.

3.3. Case Study 2: 09–10 January 2018

On 0600 UTC 09 January 2018 (DOY = 9.25), the ship was located at −50.4173°S, 137.225°E, traveling toward the Hobart. The MWACR sampled an ~30-hr segment of MBL clouds. Backward trajectories (Figure 7) show that the MBLs experienced distinctive LLWAA in the first half of the period. After DOY = 9.75, the LLWAA starts to weaken and shifts to neutral and weakly cold temperature advections.

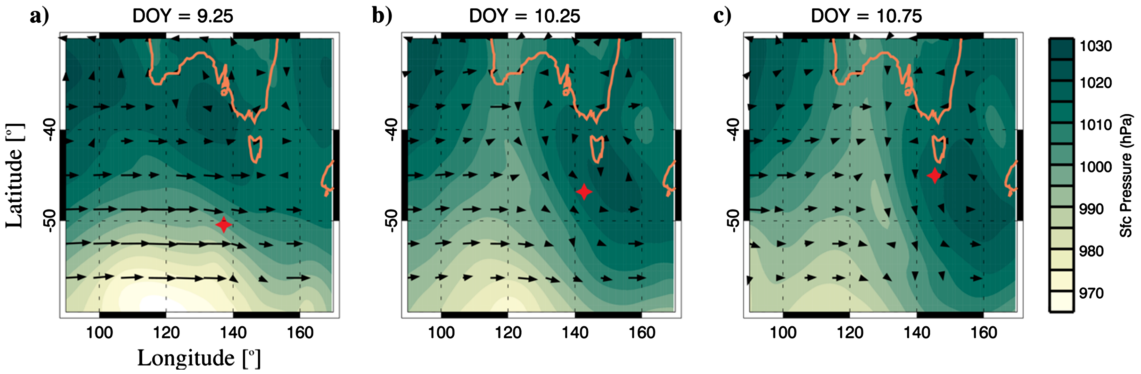

Figure 8. Same with Figure 3 but for (a) DOY = 9.25, (b) 10.25, and (c) 10.75.

Although the shift of the thermal advection is not as distinctive as that in first case, it is still instructive to compare the MBL and cloud properties between the first and second half of the period.

Figure 8a shows the synoptic map at DOY = 9.25. Unlike the first case under the influence of cold front passage, there is no sharply defined frontal system. The ship was located near southern frank of a high-pressure system and underwent northwesterly winds. Consistent with the synoptic meteorological field, a northwest-southeast swath of low-level clouds is noticeable from the satellite imagery (Figure 9a), suggesting that the clouds were advected polarward with decreasing underlying SST. After one day, the high-pressure system moved southeastward with the center locating near −45°S, 150°E. The ship moved northeastward toward the high-pressure center and stayed close to the center for the rest of the period (Figures 8b and 8c). Under the influence of the strong large-scale subsidence of the high-pressure system, the clouds above the ship were drying out near the end of the period, as seen from the infrared satellite image (Figure 9c) and the ship-borne MWACR image (Figure 10a).

Shipborne observations (Figure 10a) show a marked change of MBL structure over time: from a deep MBL within which two layers of stratiform clouds embedded to a relatively shallower MBL with clusters of cumulus underneath a stratocumulus deck. The change of the MBL structure is in-sync with a change of the temperature advection that is initially positive, and shifts to negative in the end. The distinctive LLWAA period (marked by pink shadings) shows a picture that is consistent with our hypothesis of LLWAA causing MBL decoupling: SST smaller than the T_{air} (Figure 10c) and highly stratified MBL (Figures 10a and 10b). The MWACR suggests a double-layer-stratiform-cloud structure: a cloud anvil topped by the main inversion and a near-surface cloud layer rooted in the surface mixed layer. Note that such a double-layer-cloud structure is different from the cumulus-fed stratocumulus as typical in LLCAA conditions. The distinction is that the lower cloud layer in this case manifests stratiform (marked by a red arrow in Figure 10a), not cumuliform. There are continuous (not random) occurrences of clouds as shown by the ceilometer measurements (black points) near DOY = 9.5. The presence of two stratiform

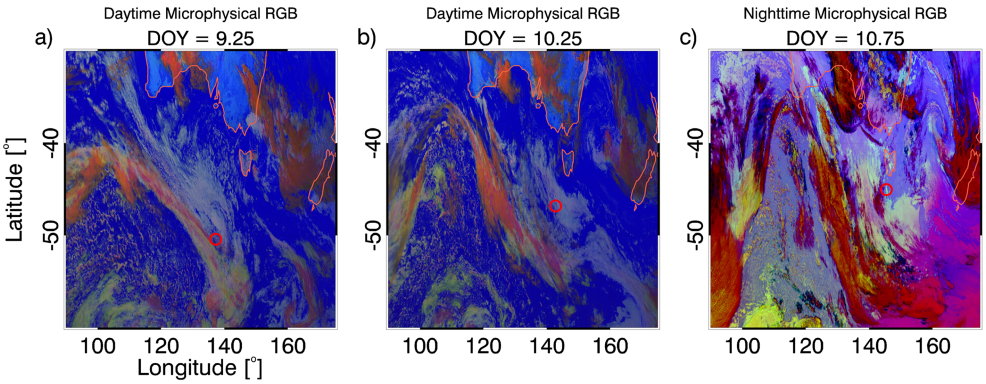

Figure 9. Same with Figure 4 but for DOY = 9.25–10.5.

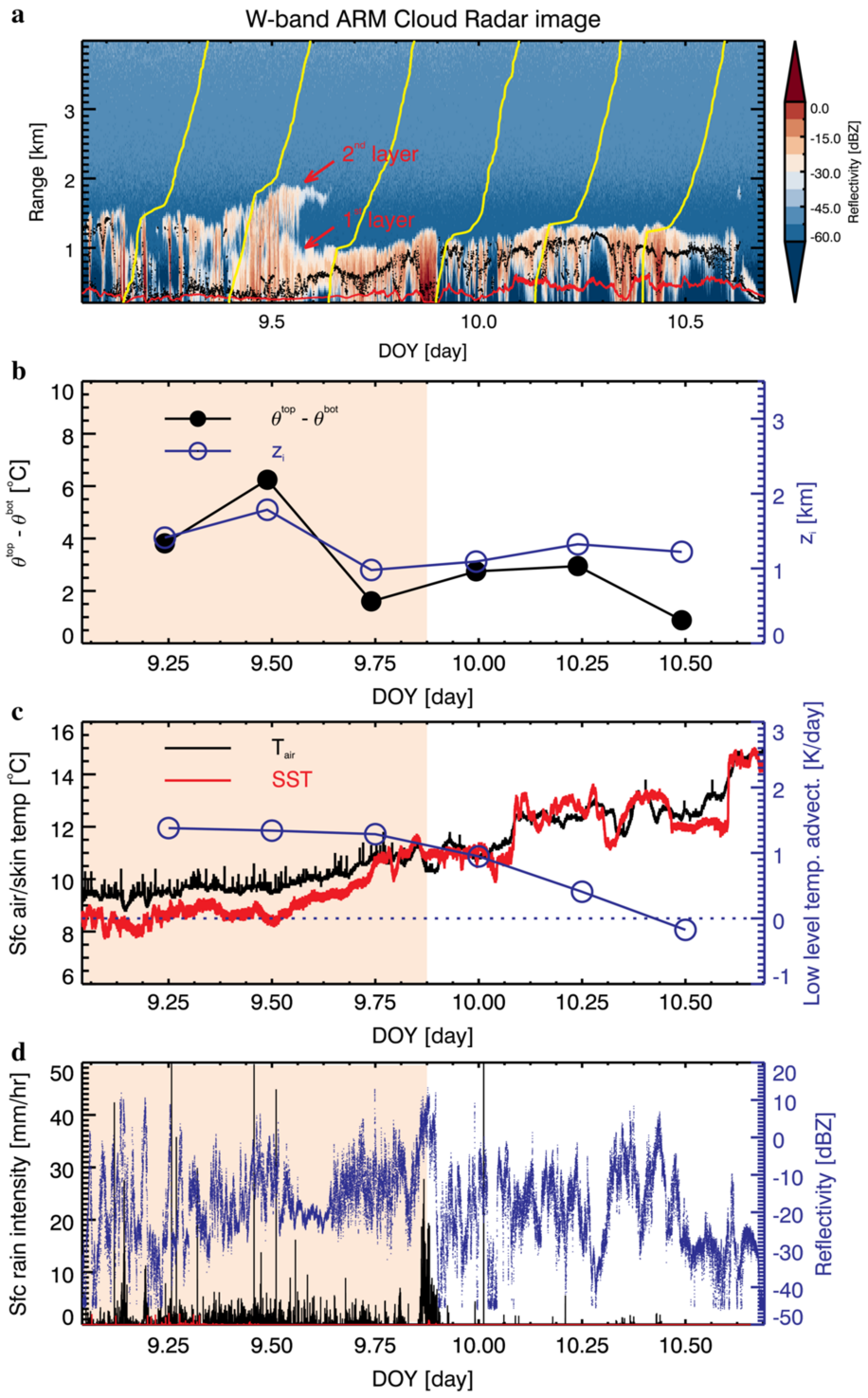

Figure 10. Same with Figure 6 but for DOY = 9.25–10.5.

cloud layers is also suggested by the radiosonde data at DOY = 9.5 (red lines in Figure 11b) that show two distinctive saturated layers.

Although we cannot guarantee that the LLWAA-induced stratification is the sole cause of the stratiform structure of the lower cloud layer, the LLWAA should certainly contribute to the its formation. As shown

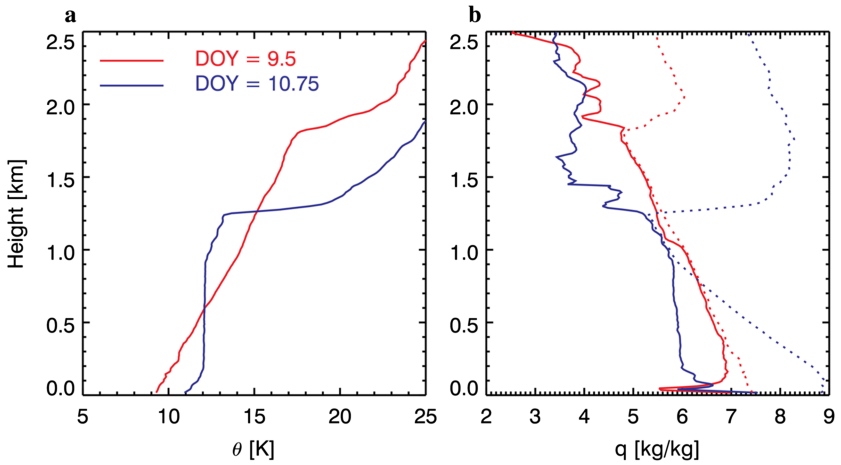

Figure 11. Profiles of (a) θ and (b) q for DOY = 9.25 (red) and 10.75 (blue). The dashed lines in (b) represent the saturation water vapor mixing ratio.

by the radiosonde data (left two yellow lines in Figure 10a), the stratification is already distinctive as low as several hundreds of meters above the sea. The stable layer favors the formation of clouds by trapping the moisture (Klein & Hartmann, 1993; Wood & Bretherton, 2006). Comparison of the thermodynamic soundings between the DOY = 9.5 and DOY = 10.5 when the temperature advection is weakly positive shows a contrast in the mixing degree of the MBL (Figure 11). The sounding at DOY = 9.5 is markedly more stratified than that at DOY = 10.5 in particular below 0.5 km, which matches the altitudes of the lower cloud layer. Note that there is also a weak inversion below 0.2 km at DOY = 10.5. This may be due to cold pools induced by the shafts of precipitation near the sounding time. Jensen et al. (2000) found that the θ can be depressed by more than 1° in the cold pools over the Southern Ocean region. The q profile shows an increase in q below 200 m, which is consistent with evaporation of rain drops moistening the ambient air (Terai & Wood, 2013). Another explanation for the temperature inversion below 200 m is the inverse "*V*" shape of the backward trajectory (Figure 7) for air mass at DOY = 10.5. Unlike previous air parcels that experience near uniform decrease or increase in SST, the air masses at DOY = 10.5 experienced increasing-then-decreasing of SST during the 36 hr in the history. The weak LLWAA before the air masses went through the region caused such a weak near-surface inversion, although the MBL is overall well mixed. Temperature inversion traps the moisture, humidifying the layer below the inversion.

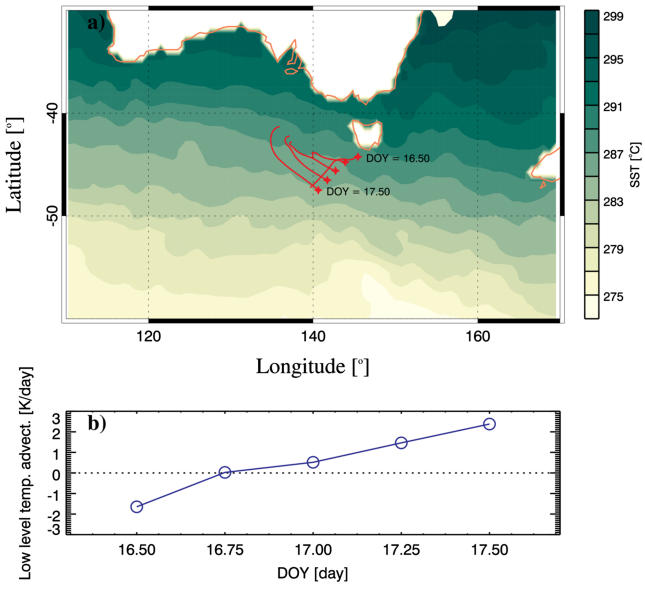

Figure 12. Same with Figure 2 but for DOY = 16.5–17.5.

An interesting aspect of this case is that the more decoupled MBLs are associated with stronger surface precipitation (Figure 10d). This is likely due to the formation of a lower cloud layer, precipitation from which is easier to reach the surface because the rain drops experience less evaporation. The time series of the maximum radar reflectivity in the vertical, as an effective proxy for precipitation at cloud bases (Comstock et al., 2004), do not show any marked change throughout the period. This indicates that the precipitation generated by the clouds does not change much, so the contrast in surface precipitation is likely due to difference in the lowest cloud base height. It has been well known that the surface precipitation rate has a significant impact on the moist and energy budget of a MBL (Nicholls, 1984; Wood, 2007). Stronger surface precipitation stabilizes a subcloud layer, weakens the TKE of the MBL, decreases the cloud-top entrainment rate, and, as a result, buffers the entrainment-induced dissipation of the clouds. This is an important process complicating the quantification of the aerosol lifetime effect, which has been hindering our understanding of the role of aerosol in

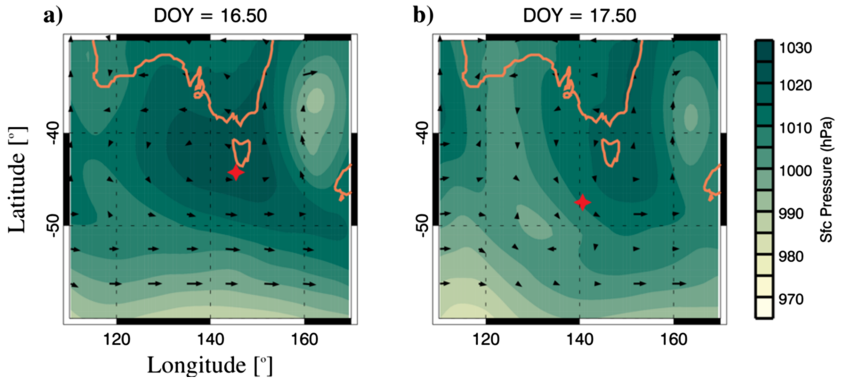

Figure 13. Same with Figure 3 but for DOY = (a) 16.5 and (b) 17.5.

altering cloud properties (Stevens & Feingold, 2009; Wood, 2007). Our results highlight the potentially significant role of LLWAA in regulating surface precipitation: it stabilizes a MBL, favoring the formation of lower clouds, from which the precipitation is more likely to reach the surface.

3.4. Case study 3: 16–17 January 2018

On 1200 UTC 16 January 2018, the *Aurora Australis* was departing from the Hobart toward polar sites. The direction of the ship is opposite to the previous two cases. During this ~24-hr period, the low-level thermal advection of the region shifted from the cold to warm temperature advection (Figure 12). The direction of the shift is also opposite to the previous two cases. The reanalysis synoptic meteorology (Figure 13) shows that the ship was initially located near the high-pressure center and then moved to the southwestern edge of the system that remains stagnant during the period. The synoptic setting is very similar to the second case but the ship travelled in an opposite direction.

Figure 14 shows the ship observations during this period. The radiosonde data in the first 12 hr and the infrared thermometer SST measurements were missed. For SST, we use the reanalysis SST data instead to examine the temperature difference between the near-surface air and the sea surfaces (Figure 14c). Consistent with the findings from the last two cases, the stratification of MBL and the temperature gradient near surface show strong dependence on the thermal advections: LLWAA is associated with more negative surface temperature gradients (Figure 14c) and more stratified MBLs (Figures 14a and 14b).

This case also illustrates the importance of large-scale subsidence in drying out the marine low clouds. The clouds before DOY = 17 were closer to the high-pressure center, undergoing strong large-scale subsidence. On one hand, the subsidence enhances the cloud-top radiative cooling by drying out the free-troposphere and allowing more exposure of the clouds to the cold space. Stronger radiative cooling enhances the turbulent mixing of the MBL, increasing the moisture transport. On the other, the subsidence-induced drying can desiccate the MBL, thinning the clouds. At least in this case, the second effect appears to outweigh the first one. This could be seen from the thinner and less precipitating clouds before DOY = 17 compared with those after DOY = 17 (Figures 14a and 14d), although the latter are more decoupled from the surface. There is no signature of diurnal cycle of MBL coupling state and cloud thickness so that the diurnal decoupling is unlikely to play a role here.

4. Discussion and Implications

The above case studies reveal several common characteristics of cloud-topped MBL under the influence of the LLWAA: (1) near-surface temperature 1 or 2 K higher than the SST, indicative of negative surface heat fluxes, (2) thermodynamically stratified (or "decoupled" in a traditional sense) MBLs, (3) stratiform clouds with visible reflectances of ~0.15 to 0.25 pending on their stages of a life cycle, and (4) occurring in warm sector of cyclones. Key statistics of the LLWAA cases with $-\overline{\frac{dSST}{dt}}>1$ K/day are summarized in Table S1. Here we discuss three relevant problems that may be shed light upon by the findings.

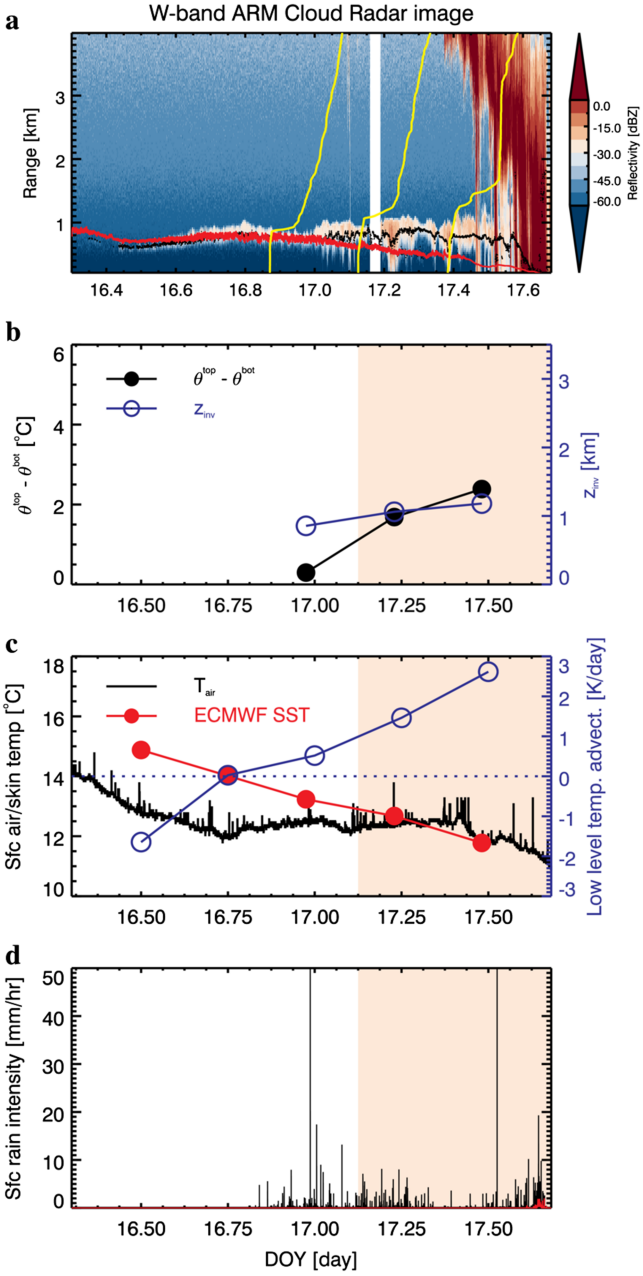

Figure 14. Same with Figure 6 but for DOY = 16.5–17.5.

4.1. Implication for passive satellite estimation of cloud-top height

Passive satellite sensors have been used to estimate the cloud-top height (H_t) of low-lying clouds using $H_t = (SST - T_t)/\Gamma$ where the T_t and Γ stand for the cloud-top temperature and the mean lapse rate of the boundary layer, respectively. The Γ has been specified as empirically determined values. Figure 15 shows the most commonly used values of Γ. Wood and Bretherton (2004) parameterize the Γ as a function of z_{inv} using satellite and reanalysis data. Zuidema et al. (2009) did a similar parameterization but using ship-based meteorological data and radiosonde measurements. Values from Minnis et al. (1992) and Stevens et al. (2007) are both from aircraft soundings. All of these empirical values are obtained from tropical or subtropical regions. Here we collect the LLWAA samples ($-\overline{\frac{dSST}{dt}} > 1$ K/day) from the MARCUS and calculate the $\Gamma = (SST - T_{inv})/z_{inv}$, in which the T_{inv} and z_{inv} are used to approximate the T_t and H_t, respectively. As shown in the Figure 15, the Γ of the LLWAA cases (black filled symbols) are markedly lower than the subtropical values except one point from the third case. The lower Γ are partially contributed by the stability across the surface layer ($SST < T_{air}$). If we use the T_{air} to replace SST in the Γ calculation, the Γ (open black symbols) are still systematically lower than the subtropical values (T_{air} may be low biased by the occurrence of cold pools, but they are not detected for the LLWAA cases surveyed in this study). This means that the boundary layer fluids are still markedly more stable in LLWAA conditions even if the stability caused by the negative surface-air temperature difference is not accounted for.

The results here show that the conventional Γ used for estimating the H_t of marine low clouds are overestimated in a LLWAA environment. This may cause an underestimation of H_t. For a LLWAA MBL with z_{inv} of 1.5 km and Γ = 6.5 K/km, an underestimation in H_t ranges from ~100 m (Minnis et al., 1992) to ~350 m (Wood & Bretherton, 2004).

4.2. What determines the life cycle of a decoupled Sc under LLWAA?

It has always been challenging to track the life cycle of clouds, in particular to identify when and where the clouds are formed. In addition, most of the clouds surveyed in this study were, during some periods, overlain by extensive high cloud layers along the ±24-hr track of the air masses, prohibiting a detailed Lagrangian analysis of their life cycles. Here we select one case sampled at the 12 UTC 09 January, which was least influenced by the high-cloud shadings along its ±24-hr track. The air mass was advected southward during the majority of the time, suggesting a LLWAA. As shown by the Animation S2, the cloud fractional coverage maintained extensive throughout the majority of the 48-hr period, indicating a possible longevity at least for this case.

Here we discuss some of the possible influential factors (both dynamic and thermodynamic factors) that can modulate the life cycle of a decoupled Sc under the LLWAA:

5. Synoptic setting

The LLWAA typically occurs ahead of cold fronts or in warm sector of cyclones. These regions are characterized by large-scale ascent or weakly descent motions. According to the quasi-geostrophic omega equation (Holton, 1973), the LLWAA contributes to large-scale ascent because of the differential heating in the

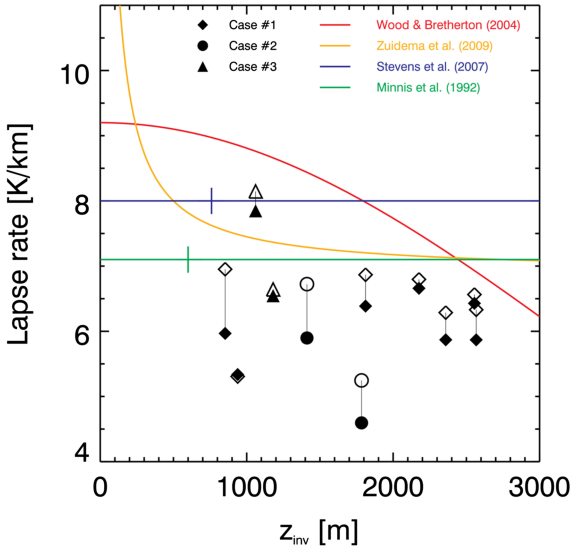

Figure 15. Lapse rate of MBL as a function of z_{inv} from various previous studies and data samples under LLWAA in this study. For Stevens et al. (2007) and Minnis et al. (1992), the lapse rates are climatological mean values and are independent of z_{inv}, we use the short vertical lines to mark the corresponding mean z_{inv}. The filled and open symbols stand for the lapse rate calculated using SST and T_{air}, respectively.

vertical (high-level temperature advection is typically negligible). This means that the decoupled clouds associated with the LLWAA are at least free from the subsidence-induced drying. This effect is mostly pronounced in the case #3. When the ship travelled from the high-pressure center to the margins, the sampled clouds are thicker and more drizzling even though the MBL is more decoupled due to the LLWAA. The absence of considerable subsidence drying may contribute to prolonging the lifetime of decoupled clouds under the LLWAA.

5.1. Frontal lifting

An LLWAA episode can also be considered as a weak warm front. The frontal lifting elevates the cloud layers, which, on one hand, strengthens the decoupling, and, on the other hand, helps sustain the condensates. The combined effect on the cloud lifetime is still unknown with the data sets used in the present study. The biggest challenge is the difficulty of separating the effects of frontal lifting and the synoptic-scale dynamic lifting. While the later can be diagnosed from the synoptic weather map from reanalysis data, the degree of the kinetic lifting is more challenging to obtain. We leave this as an open question for future research.

5.2. Convection and entrainment

Ventilation of Sc decks with free-tropospheric dry air is one of the most important processes drying out the clouds. The entrainment rate is largely dependent on the turbulence level in the clouds (Stevens, 2002). Stronger convection, on one hand, feeds more moisture to the clouds, and, on the other hand, consumes more cloud water via enhancing the entrainment drying. In a decoupled cloud regime, the clouds are more quiescent (Zheng et al., 2016). The lower turbulence level weakens the entrainment rate, sustaining the clouds against dissipation. Although the clouds will eventually decay due to the lack of the moisture supply, its lifetime could be long (several tens of hours as shown in the Animation S2) due to such a negative feedback.

It is instructive to compare this maintenance mechanism of decoupled clouds under LLWAA with that of LLCAA. The LLCAA allows for a conditionally unstable environment that is favorable for the vertical growth of cumulus clouds underneath the decoupled the Sc decks (Bretherton, 1997; Miller & Albrecht, 1995; Zheng et al., 2018a). Although these cumulus clouds can help sustain the stratocumulus decks by transporting moisture to the upper level (Jensen et al., 2000; Miller & Albrecht, 1995; Zheng et al., 2018b), once the cumulus clouds become vigorous enough, they penetrate through the overlying Sc decks and cause strong ventilation that is effective at drying out the Sc decks (Bretherton, 1997). In the meantime, the deep cumulus generates strong precipitation that may reach the ground, forming gust fronts. Interactions between gust fronts in a mesoscale MBL cloud system can enhance MBL circulations that breakup the Sc decks (*D* Rosenfeld et al., 2006). By either way, the enhanced entrainment rate is a key process for the dissipation of subtropical Sc sheets. These mechanisms appear to be absent in the LLWAA-induced decoupled MBLs because the strong stratification suppresses the vertical development of cumulus clouds. As shown in the three cases surveyed in this study, deep cumulus clouds penetrating the Sc decks are not observed during the LLWAA period.

5.2.1. Implication for aerosol-cloud-precipitation interactions

In a highly stratified MBL, the surface-generated aerosols may not reach the cloud bases as easily as in well-mixed conditions. Unlike subtropical decoupled MBLs in which the Sc decks are fed aerosols through the conduit of cumulus convections (Miller & Albrecht, 1995), the LLWAA-decoupled clouds should be more isolated from the surface CCN sources as long as the mechanically driven mixing due to wind shear (Chubb et al., 2016) is not strong.

As discussed in the last section, a unique feature of the LLWAA-decoupled clouds is that they are associated with specific synoptic-scale settings. Warm fronts have been found to be associated with slantwise convection (Balasubramanian & Yau, 1994), which may provide a pathway for transporting the aerosols.

Moreover, precipitation has been considered as a key modulator of CCN budget of a MBL (Wood et al., 2012) because of its scavenging effects. Conventionally, precipitation from MBL clouds in warm sectors of midlatitude cycles is considered as weaker than that in cold sectors (Stephen Klein, 2019, *personal communication*). Our radar observations show that precipitation (column maximum radar reflectivity >−17 dBZ) occurs 26.6% of the time during distinctive LLWAA period, which is closer to the low end of precipitation rate spectrum of MBL clouds over subtropics (20%–40%; Leon et al., 2008; Wood et al., 2009). If precipitation is indeed weaker for LLWAA-decoupled clouds, the lack of scavenging will allow for the accumulation of CCN particles, further suppressing precipitation. Of course, this hypothesis needs to be further tested by examining the precipitation along the trajectory of cloud-containing air masses (Wood et al., 2017).

Acknowledgments
This study is supported by the Department of Energy (DOE) Atmospheric System Research program (DE-SC0018996), the NOAA JPSS program (NA15NWS4680011), and the National Science Foundation (AGS1837811). The ground-based data in this study are available from website of ARM Climate Research Facility (www.archive.arm.gov/data). The Himawari-8 data are from the Japan Aerospace Exploration Agency (ftp.ptree.jaxa.jp). The reanalysis data are obtained from European Center for Medium Range Weather Forecasts (www.ecmwf.int). The HYSPLIT model is from the NOAA Air Resources Laboratory (https://www.ready.noaa.gov/HYSPLIT). We thank Jorgen Jensen and two anonymous reviewers for their constructive comments, which considerably improve the quality of the manuscript.

References

Agee, E. M. (1987). Mesoscale cellular convection over the oceans. *Dynamics of Atmospheres and Oceans*, *10*(4), 317–341. https://doi.org/10.1016/0377-0265(87)90023-6

Balasubramanian, G., & Yau, M. (1994). Baroclinic instability in a two-layer model with parameterized slantwise convection. *Journal of the Atmospheric Sciences*, *51*(7), 971–990. https://doi.org/10.1175/1520-0469(1994)051<0971:biiatl>2.0.co;2

Boers, R., Jensen, J., & Krummel, P. (1998). Microphysical and short-wave radiative structure of stratocumulus clouds over the Southern Ocean: Summer results and seasonal differences. *Quarterly Journal of the Royal Meteorological Society*, *124*(545), 151–168. https://doi.org/10.1002/qj.49712454507

Boucher, O., Randall, D., Artaxo, P., Bretherton, C., Feingold, G., Forster, P., et al. (2013). Clouds and aerosols. In T. F. Stocker, D. Qin, G.-K. Plattner, M. Tignor, S. K. Allen, J. Doschung, A. Nauels, Y. Xia, V. Bex, & P. M. Midgley (Eds.), *Climate change 2013: the physical science basis. Contribution of Working Group I to the Fifth Assessment Report of the Intergovernmental Panel on Climate Change* (pp. 571–657). Cambridge University Press.

Bretherton, C. S. (1997). Convection in stratocumulus-topped atmospheric boundary layers. In R. K. Smith (Ed.), *The Physics and Parameterization of Moist Atmospheric Convection* (pp. 127–142). Springer.

Bretherton, C. S., & Wyant, M. C. (1997). Moisture transport, lower-tropospheric stability, and decoupling of cloud-topped boundary layers. *Journal of the Atmospheric Sciences*, *54*(1), 148–167. https://doi.org/10.1175/1520-0469(1997)054<0148:mtltsa>2.0.co;2

Carslaw, K., Lee, L., Reddington, C., Pringle, K., Rap, A., Forster, P., et al. (2013). Large contribution of natural aerosols to uncertainty in indirect forcing. *Nature*, *503*(7474), 67–71. https://doi.org/10.1038/nature12674

Chubb, T., Huang, Y., Jensen, J., Campos, T., Siems, S., & Manton, M. (2016). Observations of high droplet number concentrations in Southern Ocean boundary layer clouds. *Atmospheric Chemistry and Physics*, *16*(2), 971–987. https://doi.org/10.5194/acp-16-971-2016

Comstock, K., Wood, R., Yuter, S., & Bretherton, C. (2004). Radar observations of precipitation in and below stratocumulus clouds. *Quarterly Journal of the Royal Meteorological Society*, *130*, 2891–2918. https://doi.org/10.1256/qj.03.187

Dong, X., Schwantes, A. C., Xi, B., & Wu, P. (2015). Investigation of the marine boundary layer cloud and CCN properties under coupled and decoupled conditions over the Azores. *Journal of Geophysical Research: Atmospheres*, *120*, 6179–6191. https://doi.org/10.1002/2014JD022939

Faloona, I., Lenschow, D. H., Campos, T., Stevens, B., Van Zanten, M., Blomquist, B., et al. (2005). Observations of entrainment in eastern Pacific marine stratocumulus using three conserved scalars. *Journal of the Atmospheric Sciences*, *62*(9), 3268–3285. https://doi.org/10.1175/JAS3541.1

George, R. C., & Wood, R. (2010). Subseasonal variability of low cloud radiative properties over the southeast Pacific Ocean. *Atmospheric Chemistry and Physics*, *10*(8), 4047–4063. https://doi.org/10.5194/acp-10-4047-2010

Goren, T., Rosenfeld, D., Sourdeval, O., & Quaas, J. (2018). Satellite observations of precipitating marine stratocumulus show greater cloud fraction for decoupled clouds in comparison to coupled clouds. *Geophysical Research Letters*, *45*(10), 5126–5134. https://doi.org/10.1029/2018gl078122

Hande, L., Siems, S., Manton, M., & Belusic, D. (2012). Observations of wind shear over the Southern Ocean. *Journal of Geophysical Research*, *117*(D12). https://doi.org/10.1029/2012jd017488

Holton, J. R. (1973). An introduction to dynamic meteorology. *American Journal of Physics*, *41*(5), 752–754. https://doi.org/10.1119/1.1987371

Inoue, T. (1987). An instantaneous delineation of convective rainfall areas using split window data of NOAH-7 AVHRR. *Journal of the Meteorological Society of Japan. Ser. II*, *65*(3), 469–481. https://doi.org/10.2151/jmsj1965.65.3_469

Jensen, J. B., Lee, S., Krummel, P. B., Katzfey, J., & Gogoasa, D. (2000). Precipitation in marine cumulus and stratocumulus. Part I: Thermodynamic and dynamic observations of closed cell circulations and cumulus bands. *Atmospheric Research*, *54*(2-3), 117–155. https://doi.org/10.1016/s0169-8095(00)00040-5

Jones, C., Bretherton, C., & Leon, D. (2011). Coupled vs. decoupled boundary layers in VOCALS-REx. *Atmospheric Chemistry and Physics*, *11*(14), 7143–7153. https://doi.org/10.5194/acp-11-7143-2011

Klein, S. A., & Hartmann, D. L. (1993). The seasonal cycle of low stratiform clouds. *Journal of Climate*, *6*(8), 1587–1606. https://doi.org/10.1175/1520-0442(1993)006<1587:tscols>2.0.co;2

Lensky, I., & Rosenfeld, D. (2008). Clouds-aerosols-precipitation satellite analysis tool (CAPSAT). *Atmospheric Chemistry and Physics*, *8*(22), 6739–6753. https://doi.org/10.5194/acp-8-6739-2008

Leon, D. C., Wang, Z., & Liu, D. (2008). Climatology of drizzle in marine boundary layer clouds based on 1 year of data from CloudSat and Cloud-Aerosol Lidar and Infrared Pathfinder Satellite Observations (CALIPSO). *Journal of Geophysical Research*, *113*(D8). https://doi.org/10.1029/2008jd009835

Lilly, D. K. (1968). Models of cloud-topped mixed layers under a strong inversion. *Quarterly Journal of the Royal Meteorological Society*, *94*(401), 292–309. https://doi.org/10.1002/qj.49709440106

Luo, T., Wang, Z., Zhang, D., & Chen, B. (2016). Marine boundary layer structure as observed by A-train satellites. *Atmospheric Chemistry and Physics*, *16*(9), 5891–5903. https://doi.org/10.5194/acp-16-5891-2016

Martin, G., Johnson, D., Rogers, D., Jonas, P., Minnis, P., & Hegg, D. (1995). Observations of the interaction between cumulus clouds and warm stratocumulus clouds in the marine boundary layer during ASTEX. *Journal of the Atmospheric Sciences*, *52*(16), 2902–2922. https://doi.org/10.1175/1520-0469(1995)052<2902:ootibc>2.0.co;2

McGibbon, J., & Bretherton, C. (2017). Skill of ship-following large-eddy simulations in reproducing MAGIC observations across the northeast Pacific stratocumulus to cumulus transition region. *Journal of Advances in Modeling Earth Systems*, *9*, 810–831. https://doi.org/10.1002/2017ms000924

Miller, M. A., & Albrecht, B. A. (1995). Surface-based observations of mesoscale cumulus–stratocumulus interaction during ASTEX. *Journal of the Atmospheric Sciences*, *52*(16), 2809–2826. https://doi.org/10.1175/1520-0469(1995)052<2809:sboomc>2.0.co;2

Minnis, P., Heck, P. W., Young, D. F., Fairall, C., & Snider, J. (1992). Stratocumulus cloud properties derived from simultaneous satellite and island-based instrumentation during FIRE. *Journal of Applied Meteorology*, *31*(4), 317–339. https://doi.org/10.1175/1520-0450(1992)031<0317:scpdfs>2.0.co;2

Muhlbauer, A., McCoy, I. L., & Wood, R. (2014). Climatology of stratocumulus cloud morphologies: Microphysical properties and radiative effects. *Atmospheric Chemistry and Physics*, *14*(13), 6695–6716. https://doi.org/10.5194/acp-14-6695-2014

Nicholls, S. (1984). The dynamics of stratocumulus: Aircraft observations and comparisons with a mixed layer model. *Quarterly Journal of the Royal Meteorological Society*, *110*(466), 783–820. https://doi.org/10.1002/qj.49711046603

Norris, J. R., & Iacobellis, S. F. (2005). North Pacific cloud feedbacks inferred from synoptic-scale dynamic and thermodynamic relationships. *Journal of Climate*, *18*(22), 4862–4878. https://doi.org/10.1175/jcli3558.1

O, K.-T., Wood, R., & Tseng, H.-H. (2018). Deeper, Precipitating PBLs Associated With Optically Thin Veil Clouds in the Sc-Cu Transition. *Geophysical Research Letters*, *45*, 5177–5184. https://doi.org/10.1029/2018gl077084

Romps, D. M. (2017). Exact Expression for the Lifting Condensation Level. *Journal of the Atmospheric Sciences*, *74*(12), 3891–3900. https://doi.org/10.1175/jas-d-17-0102.1

Rosenfeld, D., Kaufman, Y., & Koren, I. (2006). Switching cloud cover and dynamical regimes from open to closed Benard cells in response to the suppression of precipitation by aerosols. *Atmospheric Chemistry and Physics*, *6*(9), 2503–2511. https://doi.org/10.5194/acp-6-2503-2006

Rosenfeld, D., & Lensky, I. M. (1998). Satellite-based insights into precipitation formation processes in continental and maritime convective clouds. *Bulletin of the American Meteorological Society*, *79*(11), 2457–2476. https://doi.org/10.1175/1520-0477(1998)079<2457:sbiipf>2.0.co;2

Russell, L. M., Lenschow, D. H., Laursen, K. K., Krummel, P. B., Siems, S. T., Bandy, A. R., et al. (1998). Bidirectional mixing in an ACE 1 marine boundary layer overlain by a second turbulent layer. *Journal of Geophysical Research*, *103*(D13), 16,411–16,432. https://doi.org/10.1029/97jd03437

Sinclair, V. A., Belcher, S. E., & Gray, S. L. (2010). Synoptic controls on boundary-layer characteristics. *Boundary-Layer Meteorology*, *134*(3), 387–409. https://doi.org/10.1007/s10546-009-9455-6

Stein, A., Draxler, R. R., Rolph, G. D., Stunder, B. J., Cohen, M., & Ngan, F. (2015). NOAA's HYSPLIT atmospheric transport and dispersion modeling system. *Bulletin of the American Meteorological Society*, *96*(12), 2059–2077. https://doi.org/10.1175/bams-d-14-00110.1

Stevens, B. (2000). Cloud transitions and decoupling in shear-free stratocumulus-topped boundary layers. *Geophysical Research Letters*, *27*(16), 2557–2560. https://doi.org/10.1029/1999gl011257

Stevens, B. (2002). Entrainment in stratocumulus-topped mixed layers. *Quarterly Journal of the Royal Meteorological Society*, *128*(586), 2663–2690. https://doi.org/10.1256/qj.01.202

Stevens, B. (2006). Bulk boundary-layer concepts for simplified models of tropical dynamics. *Theoretical and Computational Fluid Dynamics*, *20*(5-6), 279–304. https://doi.org/10.1007/s00162-006-0032-z

Stevens, B., Beljaars, A., Bordoni, S., Holloway, C., Köhler, M., Krueger, S., et al. (2007). On the structure of the lower troposphere in the summertime stratocumulus regime of the northeast Pacific. *Monthly Weather Review*, *135*(3), 985–1005. https://doi.org/10.1175/mwr3427.1

Stevens, B., & Feingold, G. (2009). Untangling aerosol effects on clouds and precipitation in a buffered system. *Nature*, *461*(7264), 607–613. https://doi.org/10.1038/nature08281

Terai, C., & Wood, R. (2013). Aircraft observations of cold pools under marine stratocumulus. *Atmospheric Chemistry and Physics*, *13*(19), 9899–9914. https://doi.org/10.5194/acp-13-9899-2013

Wall, C. J., Hartmann, D. L., & Ma, P.-L. (2017). Instantaneous linkages between clouds and large-scale meteorology over the Southern Ocean in observations and a climate model. *Journal of Climate*, *30*(23), 9455–9474. https://doi.org/10.1175/jcli-d-17-0156.1

Wood, R. (2007). Cancellation of aerosol indirect effects in marine stratocumulus through cloud thinning. *Journal of the Atmospheric Sciences*, *64*(7), 2657–2669. https://doi.org/10.1175/jas3942.1

Wood, R. (2012). Stratocumulus clouds. *Monthly Weather Review*, *140*(8), 2373–2423. https://doi.org/10.1175/mwr-d-11-00121.1

Wood, R., & Bretherton, C. S. (2004). Boundary layer depth, entrainment, and decoupling in the cloud-capped subtropical and tropical marine boundary layer. *Journal of Climate*, *17*(18), 3576–3588. https://doi.org/10.1175/1520-0442(2004)017<3576:bldead>2.0.co;2

Wood, R., & Bretherton, C. S. (2006). On the relationship between stratiform low cloud cover and lower-tropospheric stability. *Journal of Climate*, *19*(24), 6425–6432. https://doi.org/10.1175/jcli3988.1

Wood, R., Kubar, T. L., & Hartmann, D. L. (2009). Understanding the importance of microphysics and macrophysics for warm rain in marine low clouds. Part II: Heuristic models of rain formation. *Journal of the Atmospheric Sciences*, *66*(10), 2973–2990. https://doi.org/10.1175/2009jas3072.1

Wood, R., Leon, D., Lebsock, M., Snider, J., & Clarke, A. D. (2012). Precipitation driving of droplet concentration variability in marine low clouds. *Journal of Geophysical Research*, *117*(D19). https://doi.org/10.1029/2012jd018305

Wood, R., Stemmler, J. D., Rémillard, J., & Jefferson, A. (2017). Low-CCN concentration air masses over the eastern North Atlantic: Seasonality, meteorology, and drivers. *Journal of Geophysical Research: Atmospheres*, *122*, 1203–1223. https://doi.org/10.1002/2016jd025557

Xu, H., Xie, S.-P., & Wang, Y. (2005). Subseasonal variability of the southeast Pacific stratus cloud deck. *Journal of Climate*, *18*(1), 131–142. https://doi.org/10.1175/jcli3250.1

Zheng, Y., Rosenfeld, D., & Li, Z. (2016). Quantifying cloud base updraft speeds of marine stratocumulus from cloud top radiative cooling. *Geophysical Research Letters*, *43*, 11,407–11,413. https://doi.org/10.1002/2016gl071185

Zheng, Y., Rosenfeld, D., & Li, Z. (2018a). Estimating the decoupling degree of subtropical marine stratocumulus decks from satellite. *Geophysical Research Letters*, *45*(22), 12,560–12,568. https://doi.org/10.1029/2018gl078382

Zheng, Y., Rosenfeld, D., & Li, Z. (2018b). The Relationships Between Cloud Top Radiative Cooling Rates, Surface Latent Heat Fluxes, and Cloud-Base Heights in Marine Stratocumulus. *Journal of Geophysical Research: Atmospheres*, *123*(20), 11,678–611,690. https://doi.org/10.1029/2018jd028579

Zuidema, P., Painemal, D., De Szoeke, S., & Fairall, C. (2009). Stratocumulus cloud-top height estimates and their climatic implications. *Journal of Climate*, *22*(17), 4652–4666. https://doi.org/10.1175/2009jcli2708.1